

# Nanoindentation of silicon nitride: A multimillion-atom molecular dynamics study

Phillip Walsh, Andrey Omeltchenko, Rajiv K. Kalia, Aiichiro Nakano, and Priya Vashishta<sup>a)</sup>  
*Collaboratory for Advanced Computing and Simulations, Department of Materials Science and Engineering, Department of Physics and Astronomy, and Department of Computer Science, University of Southern California, Los Angeles, California 90089-0242*

Subhash Saini

*Numerical Aerospace Simulation Facility, NASA-Ames Research Center, Moffett Field, California 94035*

(Received 30 May 2002; accepted 13 November 2002)

Nanoindentation of crystalline and amorphous silicon nitride films is studied using 10-million-atom molecular dynamics simulations. A rigid pyramid-shaped indenter tip is used. Load–displacement curves are computed and are used to derive hardness and elastic moduli of the simulated crystalline and amorphous films. Computer images of local pressure distributions and configuration snapshots show that plastic deformation in the film extends to regions far from the actual indent. © 2003 American Institute of Physics. [DOI: 10.1063/1.1535263]

In a nanoindentation experiment, a hard, sharp, usually pyramid-shaped tip is forced into the surface of a material. The resulting damage is used to rank the material's hardness (its resistance to plastic deformation) and elastic modulus.<sup>1–3</sup> Nanoindentation is also used in detailed studies of tip–surface interactions.<sup>4</sup> In recent years, chemically functionalized atomic force microscope tips have been used to measure forces between biological molecules, such as biotin and streptavidin, and DNA segments.<sup>5–8</sup>

Computer simulations of nanoindentation have been used for studying atomic-scale processes typically not accessible to experiments. Small-scale molecular dynamics (MD) simulations of nanoindentation of diamond<sup>9</sup> and metals<sup>10,11</sup> have given many important insights into the nature of tip–surface adhesion and the resulting tip and surface damage. Computer simulations of pressure-induced phase transformations at small scales<sup>12,13</sup> have important implications for nanoindentation studies, since indentation processes are characterized by high, localized pressures having complicated distributions. Simulations of nanoindentation of silicon<sup>14,15</sup> have explored the mechanisms involved in phase transformations under the indenter. In general, however, previous nanoindentation simulations have not reproduced accurate hardness or elastic modulus measurements.

Due to recent advances in the sizes of MD simulations, realistic comparisons between calculated and experimental mechanical properties, such as hardness, have become conceivable. Large-scale MD simulations (10–100 million atoms, corresponding to system sizes of tens of nanometers) of ceramic and inert gas systems have already been done,<sup>16–18</sup> whereas one commonly used nanoindenting apparatus has a force resolution of  $\pm 75$  nN and a depth resolution of  $\pm 0.1$  nm.<sup>1</sup> Clearly, a direct comparison of MD results with experimental results of the same scale is already possible.

In this letter, we report 10-million-atom MD simulations of nanoindentation of crystalline and amorphous Si<sub>3</sub>N<sub>4</sub>. These simulations demonstrate the feasibility of using MD

simulations to rank material properties, such as hardness, and to improve on the quality of interatomic potentials for various materials.

Silicon nitride was described by the interatomic potential developed by Vashishta and coworkers<sup>19,20</sup> for tetrahedral-based ceramic and semiconductor materials:

$$V = \sum_{i < j} V_{ij}^{(2)} + \sum_{i < j < k} V_{jik}^{(3)}, \quad (1)$$

where

$$V_{ij}^{(2)} = \frac{A_{ij}(\sigma_i + \sigma_j)^{\eta_{ij}}}{r_{ij}^{\eta_{ij}}} + \frac{Z_i Z_j}{r_{ij}} e^{-r_{ij}/r_{1s}} - \frac{P_{ij}}{r_{ij}^4} e^{-r_{ij}/r_{4s}}, \quad (2)$$

$$P_{ij} = (\alpha_i Z_i^2 + \alpha_j Z_j^2)/2, \quad (3)$$

and

$$V_{jik}^{(3)} = B_{jik} \left( \frac{\mathbf{r}_{ik} \cdot \mathbf{r}_{ij}}{r_{ik} r_{ij}} - \cos \bar{\theta}_{jik} \right)^2 \exp \left( \frac{1}{r_{ij} - r_{c3}} + \frac{1}{r_{ik} - r_{c3}} \right). \quad (4)$$

The parameters are given in Table I.  $r_{ij}$  is the distance between atoms  $i$  and  $j$ .

The simulated  $\alpha$ -Si<sub>3</sub>N<sub>4</sub> film had lateral dimensions of 606 Å × 606 Å, a thickness of 300 Å, and consisted of 10 614 240 atoms. The film was oriented so the indent was done into a free (0001)  $\alpha$ -Si<sub>3</sub>N<sub>4</sub> surface. The  $x$  and  $y$  simulation cell walls were normal to the (10 $\bar{1}$ 0) and ( $\bar{1}$ 2 $\bar{1}$ 0) surfaces, respectively. Periodic boundary conditions were used in the  $x$  and  $y$  directions. Amorphous Si<sub>3</sub>N<sub>4</sub> was prepared by heating bulk  $\alpha$ -Si<sub>3</sub>N<sub>4</sub> (density 3.2 g/cc) to 4500 K,

TABLE I. Si<sub>3</sub>N<sub>4</sub> parameters.

$A_{ij}$ (erg)	$r_{1s}$ (Å)	$r_{4s}$ (Å)	$r_c$ (Å)	$r_{c3}$ (Å)		Si–Si	Si–N	N–N
$2 \times 10^{-12}$	2.5	2.5	5.5	2.6	$\eta_{ij}$	11	9	7
	$\sigma_i$ (Å)	$Z_i$ (e)	$\alpha_i$ (Å <sup>3</sup> )			$B_{jik}$ (erg)	$\bar{\theta}_{jik}$	
Si	0.47	1.472	0	Si–N–Si	$2 \times 10^{-11}$	120		
N	1.30	–1.104	3	N–Si–N	$1 \times 10^{-11}$	109.47		

<sup>a)</sup>Electronic mail: priyav@usc.edu

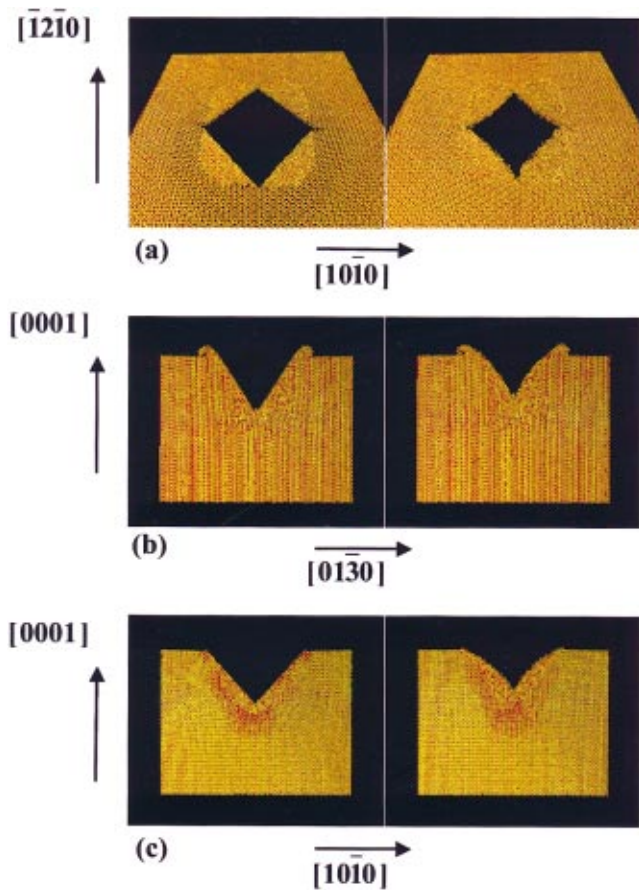


FIG. 1. (Color) Configuration views of (a) film surface, (b) slice parallel to the edges of the indenter, and (c) slice across the indenter diagonal. The left frames show fully loaded configurations while unloaded configurations are on the right.

thermalizing the liquid for 18 000 time steps (1 time step = 1 fs), and slowly quenching the liquid over 40 000 steps to form an amorphous solid.

The method of Langevin dynamics<sup>21</sup> was used to control the temperature throughout the simulation. In this method, a fictitious viscous force dissipates excess kinetic energy from the system at a rate determined by a time constant  $\tau$ . This method has the advantage of achieving spatially uniform temperature, and shorter thermalization periods are required

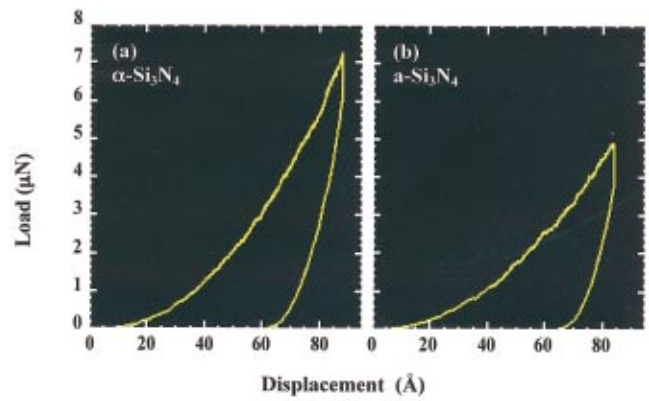


FIG. 3. (Color) Load–displacement curve for (a) 10-million-atom  $\alpha$ - $\text{Si}_3\text{N}_4$  nanoindentation simulation and (b) 10-million-atom  $a$ - $\text{Si}_3\text{N}_4$  simulation.

than with simpler scaling methods. A  $\tau$  of 400 fs was used during the amorphization schedule just described.

The indenter was a square-based pyramid having a height of 90 Å and an apex corner angle of 90°. The indenter was not allowed to deform during the simulation, that is, the indenter was infinitely hard. In addition, only repulsive interactions were allowed between the indenter and surface atoms. These simulations may be thought of as an attempt to model “ideal” experimental conditions.

After relaxing the free surface using a  $\tau$  of 100 fs, the temperature of the film was gradually increased to 300 K, followed by a short thermalization with  $\tau=200$  fs. Starting at 10 Å above the film surface, the indenter was displaced continuously at a rate of 100 m/s (the speed of sound in silicon nitride is  $\sim 7\,000$  m/s). The indenter was displaced to 90 Å, after which a 2-ps equilibration period was inserted to allow transient forces to dissipate. The indenter was then removed from the surface at the same rate. The load on the indenter was monitored throughout the simulation. The local pressure distribution was calculated every few hundred time steps as described subsequently.

Figure 1(a) shows a sequence of atomic configurations from a perspective directly above the indent. Figure 1(b) shows the same sequence for a slice under the indenter edges. Figure 1(c) shows a slice under the corners of the indenter. For clarity of presentation, the indenter atoms are

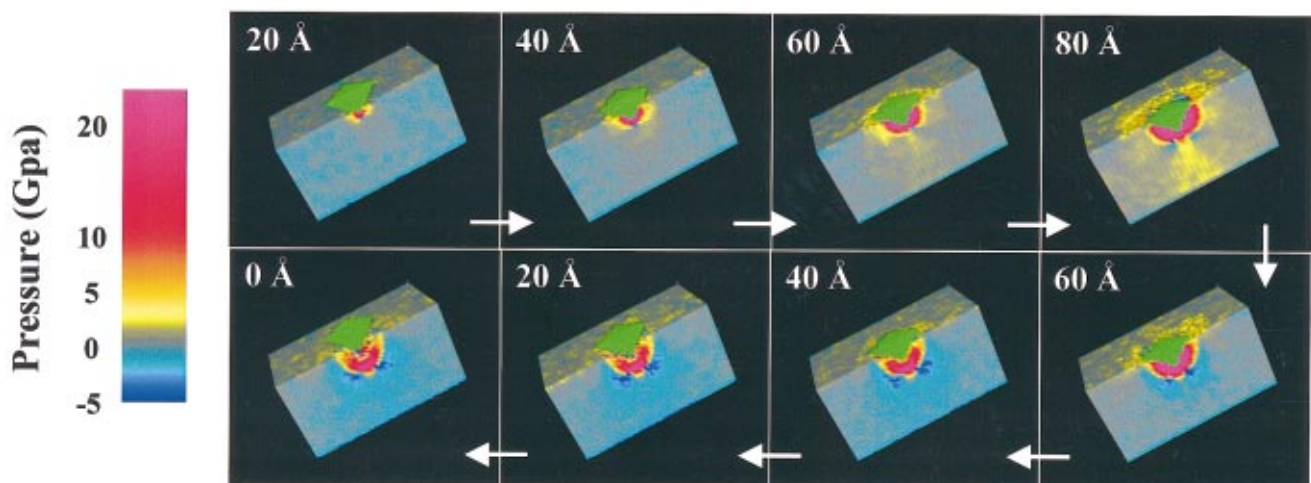


FIG. 2. (Color) Local pressure distribution directly under the indenter. Frames from the loading and unloading cycles are shown in clockwise order. The displacement of the indenter is given in the top left corner of each frame.

not included in these figures. A large amount of piled-up material is visible on the surface of the film. The piled-up material lies mostly along the edges of the indenter and is suppressed near the corners. In addition, small cracks are visible at the corners of the indenter in the fully loaded configuration. The fully unloaded configuration shows that a significant amount of elastic recovery has occurred.

The local pressure (sum of diagonal components of the stress tensor) was computed by dividing the simulation space into  $10 \times 10 \times 10 \text{ \AA}^3$  cells and calculating the stress tensor for each cell from the virial expression.<sup>22</sup> Figure 2 shows a half-slice of the local pressure distribution at various phases of the indentation process. Blue colors (light and dark) represent tensile pressures, while yellows and reds correspond to compressive pressures. The hemispherical region of high compressive pressures around the indenter tip corresponds to plastic deformation in the crystalline silicon nitride surface and includes the visible area of the indent (a pyramid-shaped divot left behind after unloading). Regions of lesser compressive pressures are observed farther from the indent, and these regions recover after unloading. This corresponds to the elastic response of the  $\text{Si}_3\text{N}_4$  film, and leads to a finite slope in unloading curves.

Figure 2 also shows regions of residual tensile pressure during unloading, showing that plastic deformation extends to a significant distance beyond the area contacted by the indenter. The tensile regions correspond to cracks originating at the surface and extending throughout the depth of the indent. A detailed analysis of the nature of the plastic deformation caused by the indenter will be presented elsewhere.

Figures 3(a) and 3(b) show the load–displacement curves for the crystalline and amorphous  $\text{Si}_3\text{N}_4$  nanoindentation simulations. The load is defined as the total force on the indenter, and displacement is measured from the indenter's starting position. Hardness values for  $\alpha$ - $\text{Si}_3\text{N}_4$  and amorphous (a)- $\text{Si}_3\text{N}_4$  were estimated by dividing the maximum relaxed load by the projected area of the indent. These hardness values are 50.3 GPa for  $\alpha$ - $\text{Si}_3\text{N}_4$  and 31.5 GPa for a- $\text{Si}_3\text{N}_4$ . The elastic moduli were estimated from the initial slopes of the unloading curves and agree with the bulk values for this potential (approximately 400 GPa for  $\alpha$ - $\text{Si}_3\text{N}_4$  and 290 GPa for a- $\text{Si}_3\text{N}_4$ ).

Values for Vickers microindentation of single-crystal  $\alpha$ - $\text{Si}_3\text{N}_4$  in the literature vary somewhat, probably due to the well-known indentation size effect (ISE). Suematsu *et al.*, who in their tests used a 300-g maximum load, give a hardness value close to 31 GPa for the (0001) surface.<sup>23</sup> Chakraborty and Mukerji report  $\alpha$ - $\text{Si}_3\text{N}_4$  hardness of 40 GPa for a 200-g load and 48 GPa for a 100-g load, where the values are averages over several different surfaces.<sup>24</sup> In converting Vickers microhardness numbers, we have multiplied by the additional factor 2/1.854, since Vickers hardness is defined by the maximum load divided by the total contact area instead of by the projected area.<sup>25</sup> We were unable to find experimental hardness values in the literature for a- $\text{Si}_3\text{N}_4$ . The ratio of a- $\text{Si}_3\text{N}_4$  hardness to  $\alpha$ - $\text{Si}_3\text{N}_4$  (0001) hardness estimated from these simulations is 0.63.

Systematic studies of the ISE for commercial grades of silicon nitride exist in the literature, but none for single-crystal silicon nitride. Still, we think that it is reasonable to

compare our hardness estimates with the higher of the experimental values. As such, we know of no other MD simulation that approaches this degree of accuracy in estimating hardness of a real material.

The simulations reported in this letter have demonstrated the feasibility of using the molecular dynamics method to study the processes involved in nanoindentation of ceramic materials. Significant pile-up is observed on the film surface, and cracks extend throughout the depth of the indent. Hardness values estimated in these simulations are very reasonable in light of Vickers microhardness values.

We believe that similar simulations of gallium arsenide, silicon carbide, and aluminum oxide will allow us to construct a hardness scale for ranking materials using MD simulations. A test of this scale will consist of comparing the relative hardness ratios of these materials with ratios inferred from existing hardness tables.

This work was supported by NASA-Ames Research Center, NSF, U.S. DOE, Army Research Laboratory, and USC–Berkeley–Princeton DURINT. Simulations were performed using DoD super computers under a DoD Challenge project.

<sup>1</sup>B. Bhushan, in *Handbook of Micro/Nano Tribology*, edited by B. Bhushan (CRC Press, New York, 1995), p. 321.

<sup>2</sup>H. M. Pollock, in *Friction, Lubrication, and Wear Technology*, edited by P. J. Blau (ASM Int'l., Materials Park, Ohio, 1992), Vol. 18, p. 419.

<sup>3</sup>V. Tikare and A. H. Heuer, *J. Am. Ceram. Soc.* **74**, 593 (1991).

<sup>4</sup>N. A. Burnham and R. J. Colton, *J. Vac. Sci. Technol. A* **7**, 2906 (1989).

<sup>5</sup>A. Noy, D. V. Vezenov, and C. M. Lieber, *Annu. Rev. Mater. Sci.* **27**, 381 (1997).

<sup>6</sup>G. U. Lee, D. A. Kidwell, and R. J. Colton, *Langmuir* **10**, 354 (1994).

<sup>7</sup>R. McKendry, M.-E. Theoclitou, T. Rayment, and C. Abell, *Nature (London)* **391**, 566 (1998).

<sup>8</sup>G. U. Lee, L. A. Chrisey, and R. J. Colton, *Science* **266**, 771 (1994).

<sup>9</sup>J. A. Harrison, C. T. White, R. J. Colton, and D. W. Brenner, *Surf. Sci.* **271**, 57 (1992).

<sup>10</sup>J. Belak, D. B. Boercker, and I. F. Stowers, *Mater. Res. Soc. Bull.* **18**(5), 55 (1993).

<sup>11</sup>U. Landman, W. D. Luedtke, N. A. Burnham, and R. J. Colton, *Science* **248**, 454 (1990).

<sup>12</sup>N. Binggeli and J. R. Chelikowsky, *Phys. Rev. Lett.* **69**, 2220 (1992).

<sup>13</sup>R. M. Wentzcovitch, C. da Silva, and J. R. Chelikowsky, *Phys. Rev. Lett.* **80**, 2149 (1998).

<sup>14</sup>G. S. Smith, E. B. Tadmor, and Efthimios Kaxiras, *Phys. Rev. Lett.* **84**, 1260 (2000).

<sup>15</sup>J. S. Kallman, W. G. Hoover, C. G. Hoover, A. J. De Groot, S. M. Lee, and F. Wooten, *Phys. Rev. B* **47**, 7705 (1993).

<sup>16</sup>F. F. Abraham, D. Schneider, B. Land, D. Lifka, J. Skovira, J. Gerner, and M. Rosenkrantz, *J. Mech. Phys. Solids* **45**, 1461 (1997).

<sup>17</sup>A. Omeltchenko, M. E. Bachlechner, A. Nakano, R. K. Kalia, P. Vashishta, I. Ebbsjö, A. Madhukar, and P. Messina, *Phys. Rev. Lett.* **84**, 318 (2000).

<sup>18</sup>M. E. Bachlechner, A. Omeltchenko, A. Nakano, R. K. Kalia, and P. Vashishta, *Appl. Phys. Lett.* **72**, 1969 (1998).

<sup>19</sup>P. Vashishta, R. K. Kalia, A. Nakano, W. Li, and I. Ebbsjö, in *Amorphous Insulators and Semiconductors*, edited by M. F. Thorpe and M. I. Mitkova (Kluwer Academic, Netherlands, 1997), p. 151.

<sup>20</sup>A. Nakano, R. K. Kalia, and P. Vashishta, *Phys. Rev. Lett.* **75**, 3138 (1995).

<sup>21</sup>M. P. Allen and D. J. Tildesley, *Computer Simulation of Liquids* (Oxford University Press, New York, 1987), p. 257.

<sup>22</sup>K. S. Cheung and S. Yip, *J. Appl. Phys.* **70**, 5688 (1991).

<sup>23</sup>H. Suematsu, J. J. Petrovic, and T. E. Mitchell, *Mater. Res. Soc. Symp. Proc.* **287**, 449 (1992).

<sup>24</sup>D. Chakraborty and J. Mukerji, *J. Mater. Sci.* **15**, 3051 (1980).

<sup>25</sup>A. R. Fee, R. Segabache, and E. L. Tobolski, in *ASME Metals Handbook*, Ninth edition, edited by J. R. Davis and S. K. Refsnes (ASME, Metals Park, OH, 1985), Vol. 8, p. 90.